NASA TM X-841

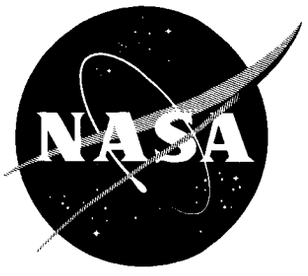

TECHNICAL MEMORANDUM

X-841

PRESSURE DISTRIBUTION AT A MACH NUMBER OF 24.5 ON A SYMMETRICAL BLUNT-FACED REENTRY BODY AT ANGLES OF ATTACK FROM 0° TO 40° IN HELIUM INCLUDING AN INVESTIGATION OF AFTERBODY STING EFFECTS

By Ralph Watson and Richard D. Wagner, Jr.

Langley Research Center
Langley Station, Hampton, Va.

NATIONAL AERONAUTICS AND SPACE ADMINISTRATION

WASHINGTON

May 1963

~~CONFIDENTIAL~~

NATIONAL AERONAUTICS AND SPACE ADMINISTRATION

TECHNICAL MEMORANDUM X-841

PRESSURE DISTRIBUTION AT A MACH NUMBER OF 24.5 ON A SYMMETRICAL BLUNT-FACED REENTRY BODY AT ANGLES OF ATTACK FROM 0° TO 40° IN HELIUM INCLUDING AN INVESTIGATION OF AFTERBODY STING EFFECTS*

By Ralph Watson and Richard D. Wagner, Jr.

SUMMARY

An experimental investigation has been conducted in the Langley 22-inch helium tunnel at a Mach number of 24.5 and a Reynolds number of 1.18×10^6 to determine the pressure distribution over the face and afterbody of a symmetrical blunt-faced reentry body at angles of attack up to 40°. Throughout the angle-of-attack range, the data on the heat shield show fair agreement with modified Newtonian theory. For angles of attack between 0° and 20°, pressures over the afterbody showed little variation with angle of attack. A value of five to ten times free-stream static pressure was measured in this angle-of-attack range; however, the results of tests to determine model-support interference effects indicate that this value is probably high.

Above an angle of attack of 20°, the afterbody pressures on the windward side rapidly increased with increasing angle of attack. Pressures on the leeward side of the afterbody experienced little change throughout the angle-of-attack range of the investigation.

INTRODUCTION

Of the many classes of reentry vehicles under consideration, the high-drag, symmetrical reentry body has received considerable attention. Thermal protection for such reentry bodies places severe weight limitations on the designer. For this reason, among others, a well-defined knowledge of aerodynamic heating is needed to make the most efficient use of thermal protection. Since the aerodynamic heating depends in part on the pressure level and distribution, an accurate knowledge of the pressures over the capsule is in turn required.

In the present investigation, tests were conducted on a typical reentry body at a Mach number of 24.5 and a Reynolds number, based on body diameter, of 1.18×10^6. Pressure distributions over a probable operational angle-of-attack

*~~Title, Unclassified.~~

~~CONFIDENTIAL~~

range were obtained to determine the pressure level and to assess the effects of angle of attack on the pressures over the face and afterbody at a Mach number typical of reentry.

In addition, the effects of sting diameter, sting length (effect of distance of model from support strut), and Mach number variation on the afterbody pressures at zero angle of attack were investigated.

SYMBOLS

$C_{p,max}$	stagnation-point pressure coefficient
d	maximum model diameter
d_s	sting diameter
L	distance from face of model to support strut at zero angle of attack
M	free-stream Mach number
p	local pressure
$p_{t,\sigma}$	stagnation pressure behind a normal shock at the stream Mach number
p_∞	free-stream static pressure
R	Reynolds number based on body diameter
s	distance measured along body surface on meridian line from stagnation point at zero angle of attack (see fig. 1)
s_d	distance measured along body surface on meridian line from stagnation point at zero angle of attack to maximum diameter point of body (see fig. 1)
α	angle of attack
ϕ	orifice ray angle (see fig. 1)

APPARATUS

Tunnel

This investigation was conducted in the Langley 22-inch helium tunnel which is described in reference 1. A schematic diagram of the tunnel, an intermittent,

closed-cycle facility, is shown in figure 2. Helium is supplied at 5,000 psig from high-pressure tanks to the stagnation chamber. The desired test stagnation pressure is controlled automatically by means of a hydraulically operated control valve. For the present tests the main body of data was obtained using a 5° half-angle conical nozzle; however, a contoured Mach number 20 nozzle was used in the interference phase of the investigation.

Downstream of the 22-inch-diameter test section, the flow passes through a two-dimensional variable-area diffuser and exhausts into two 60-foot-diameter vacuum spheres. Use of the diffuser increases the running time from approximately 40 seconds to 1 minute. The helium in the vacuum spheres is recompressed and passed through a liquid nitrogen refrigeration system and a silica gel dryer so that it contains less than 0.02 percent air by volume when it is returned to the high-pressure tanks.

Models

Models of 2.5 inches and 4 inches in maximum diameter were used in this investigation. The overall pressure distributions at angles of attack were obtained on the 4-inch-diameter model mounted on a bent sting. Each model consisted of a spherical segment heat shield joined to a conical afterbody, the vertex of which was oriented toward the rear of the model. Replacing the sharp cone vertex on the afterbody was a tangent spherical cap as shown in figure 1(a). Eighteen pressure orifices were located on the 4-inch-diameter model in a plane opposite the sting mounting hole. Fourteen of the orifices were of 0.060 inside diameter metal tubing; the other four, which were installed on the spherical cap of the afterbody cone, were 0.040 inside diameter. Test results indicated that the pressures measured on the four small diameter orifices did not settle out in the available running time and consequently are not shown in the data.

The 2.5-inch-diameter model shown in figure 1(b) was tested only at zero angle of attack and was used to investigate the effects of sting diameter and sting length on afterbody pressures. Photographs of this model and some of the stings used are shown in figure 1(c).

Instrumentation and Accuracy

Two types of pressure-measuring devices were used: diaphragm transducers on the face, and Alphatron gages on the afterbody. The diaphragm transducers produce the desired electrical output by means of a strain gage attached to the diaphragm. These gages are accurate to ± 0.04 psi, and permit an inaccuracy in pressure measurement over the heat shield of less than 4 percent in most cases.

The Alphatron gage is an ionization gage utilizing a small radioactive source to ionize a gas sample. In the range from 1 mm of Hg to 30 mm of Hg, the gage is accurate to ± 2 percent of the reading. Below 1 mm of Hg, or near ten times free-stream static pressure (p_{∞}) for the 22-inch tunnel, the accuracy is ± 5 percent of the gage reading. A characteristic of the Alphatron gage is its sensitivity to gas composition; the gages are approximately five times more

sensitive to air than to helium. For this reason extreme care was taken to eliminate all leaks and possible sources of contamination between the model orifices and the gages. Scatter in the data at extremely low pressures (below 1 mm of Hg) may be attributed to possible contamination of the sampled helium by small leaks which were otherwise undetected.

For both the conical and contoured nozzles, the Mach number was known within 1 percent. Desired flow properties can be determined by use of the tables in reference 2 and the correction factors in reference 3.

Test Conditions and Procedure

The 4-inch-diameter model (fig. 1(a)) was located in the tunnel at a station corresponding to a free-stream Mach number of 24.5 as determined from the calibration of the conical nozzle in reference 1. For the model fineness ratio of these tests, an axial Mach number gradient of 0.063 per inch in the conical nozzle was considered to have a negligible effect on the data (see ref. 4). The stagnation pressure in the settling chamber was automatically maintained at a constant value of 1,000 psig. The stagnation temperature was constant for any given test and had an average value over the tests of 500° R. These test conditions gave a Reynolds number based on body diameter of 1.18×10^6 for the large model and 1.08×10^6 for the small model at $M = 19.4$. The 2.5-inch-diameter model (fig. 1(b)) was tested at various tunnel locations by using the conical and contoured nozzles as described in the following section.

Prior to testing, the model tubes were thoroughly cleaned and outgassed because of the low pressures encountered and gas-sensitive gages used. Between tests, high-vacuum tape was placed over the orifices, and the model tubing and gages were kept under vacuum. During the tests the outputs of the transducers and Alphatron gages were recorded at 3-second intervals in order to assure that the pressures had settled out to a constant value.

RESULTS AND DISCUSSION

Sting and Tunnel Interference Effects

The 2.5-inch-diameter model (fig. 1(b)) was used to investigate possible sting-length and sting-diameter interference effects on afterbody pressures. It was necessary to shield the 4-inch-diameter model with a slender cone before flow could be established in the tunnel, and since the starting cone was fixed in the tunnel, the large model could not be moved more than about 16 inches upstream of the sting-support strut. The size of the smaller model was such that flow could be established at any tunnel position without the use of a starting cone.

The investigation of sting-diameter, d_s, and sting-length, L, effects at $\alpha = 0^{\circ}$ was conducted in three phases, two of which utilized the contoured nozzle

with a free-stream Mach number of 19.4. Use of the contoured nozzle was necessary because it was impossible to separate sting length from Mach number effects in the conical nozzle due to the conical-flow Mach number gradient. The three phases of the investigation and their results are presented in the following sections.

Sting diameter.- For a fixed sting length of $L = 22.74$ inches and $\alpha = 0^\circ$ (see fig. 3) afterbody pressures were measured on stings of various diameters such that $\frac{d_s}{d} = 0.10$, 0.15, 0.25, and 0.35 in the contoured nozzle. The results are shown in figure 4. The pressure was measured in some cases only at orifice location $\frac{s - s_d}{d} = 0.31$, since for $\frac{d_s}{d} = 0.10$ and 0.15 the internal diameter of the sting would accommodate only one pressure tube. The variation of afterbody pressure at $\frac{s - s_d}{d} = 0.31$ with $\frac{d_s}{d}$ is shown in figure 5.

The T-shaped cross-section and side-mount stings shown at the top of figure 5 were constructed of 1/64-inch steel strip to determine what sting effects might be expected for mounts of this type. The side mount presented the smallest area normal to the flow which could safely be used for the forces encountered.

No comparison in size can be made between the T-shaped sting and the offset-round sting; however, the data in figure 5 show that the lowest pressure was obtained for the smallest T sting tested. The side-mount sting produced an effect on pressure intermediate in value between the largest and smallest of the rear-mounted T stings and lower than the smallest circular sting.

It is clear that sting effects can be significant and are certainly present in the data to be presented in the following section. A more definitive evaluation of these effects than can be deduced from the data in figure 5 was not possible, since the trend is not sufficiently well established, and extrapolation of the curve to $\frac{d_s}{d} = 0$ would be unrealistic. For the value of L used, it was physically impossible to reduce appreciably the sting size below that of the smallest used in these tests.

Sting length.- With $\frac{d_s}{d}$ held constant at 0.25, afterbody pressures were determined for $L = 17.74$, 22.74, and 38.74 in the contoured nozzle. Results of this investigation are shown in figure 6 for $\frac{s - s_d}{d} = 0.31$ since all but one afterbody tube were removed while testing for sting-diameter effects.

Within the accuracy of the data, there are no effects of L on afterbody pressure for L greater than 22.74 inches. It is seen that there is a local disturbance on the tunnel center line near $L = 14.74$. The change in the level of $\frac{p}{p_\infty}$ for L less than 22.74 is believed to be caused by a contribution of both M and L effects since, as will be shown in the following section, an

increase in M with no effect attributable to L would result in an increase in the level of $\frac{p}{p_\infty}$. It is therefore concluded that for the configuration tested, sting-length effects will be negligible for $L > 22.74$ inches.

Mach number.- In the preceding two sections the extent to which changes in sting diameter and sting length affect pressures on the afterbody of the 2.5-inch-diameter model was examined at a Mach number of about 20. Since it was impossible to determine directly similar conditions for the 4-inch-diameter model at a Mach number of 24.5 in the conical nozzle, the effect of these same variables on the pressures obtained on the afterbody of the 4-inch-diameter model was assessed in the following manner. It was assumed that the minimum value of L for negligible effect on afterbody pressure obtained on the 2.5-inch-diameter model at $M = 19.4$ would also apply at the higher Mach numbers obtainable in the conical nozzle. For a fixed $\frac{d_s}{d}$ value of 0.25, afterbody pressures were then obtained for $L = 22.74$ and 32.74 with corresponding nose Mach numbers of 24 and 23 in the conical nozzle. The afterbody pressures measured at station $\frac{s - s_d}{d} = 0.31$ under these conditions along with the pressure at this same orifice obtained in the contoured nozzle at $M = 19.4$ are shown in figure 7. The linear relationship between $\frac{p}{p_\infty}$ and M may be due to either a direct effect of Mach number change on the afterbody pressure or a magnification of sting effects due to Mach number change. When this curve is extrapolated to $M = 24.5$, a value of $\frac{p}{p_\infty} = 12.4$ is obtained. This was taken to be the value of $\frac{p}{p_\infty}$ to be expected at $M = 24.5$ for negligible sting-length effects with $\frac{d_s}{d} = 0.25$.

It is clear from the partial sting-diameter effects evaluation shown in figure 5 that this value is higher than the true value (i.e., the value which would be obtained in the absence of a sting). The value of $\frac{p}{p_\infty}$ measured on the 4-inch-diameter model at station $\frac{s - s_d}{d} = 0.30$ with $L = 16.02$ was 11.3 which is about 9 percent lower than obtained by extrapolating the data for the 2.5-inch-diameter model, and is thus probably closer to the true value. Some of the factors which may account for the difference in pressure level are (a) different sting arrangement (compare figs. 1(a) and 1(b)), (b) scale effects due to model size, and (c) the 4-inch-diameter model was at less than the minimum value of L as determined from tests on the 2.5-inch model.

In any event, there are sting effects present in the afterbody data to be presented in the following section, and although these effects are of an undetermined magnitude, it seems clear that the pressures are conservative, that is, higher than the true value. This statement is felt to apply only to the low angle-of-attack range where the flow over the orifices is believed to be separated.

The results presented in this section demonstrate that support-interference effects must be more fully investigated and techniques to eliminate, or aid in their quantitative evaluation, must be developed.

Pressure Distribution at Angles of Attack

Figure 8 shows schlieren photographs of the model at four of the angles of attack of the tests.

The pressure distribution over the heat shield at zero angle of attack is presented in figure 9 and the data at angles of attack in figure 10. The data are presented as the ratio of the local pressure to the measured stagnation-point pressure at zero angle of attack. The data show fair agreement with modified Newtonian theory $\left(C_{p,max} = 1.76\right)$ but indicate a strong pressure-relieving effect near the heat-shield corner throughout the angle-of-attack range of the tests. Similar results were obtained at a Mach number of 6 for the same configuration (see ref. 5). In most cases the pressures are well below the Newtonian prediction near the heat-shield corner. In addition, the geometric stagnation point, indicated by Newtonian theory in figure 10, is seen to lead the point of maximum pressure at the higher angles of attack.

In figure 11 the measured pressure distribution on the model afterbody is shown at the various angles of attack for four roll angles. The measured pressures are shown in terms of a ratio of local pressure to free-stream static pressure against distance along the afterbody surface.

The pressure obtained on the afterbody of the present model may seem high when compared with afterbody pressures obtained on similar configurations at supersonic Mach numbers. For example, the results of reference 6 indicate that base pressures at low supersonic Mach numbers are on the order of 0.4 to 0.5 stream static pressure. However, the data of the present investigation corroborate the results of reference 7 in which it was shown by theoretical estimates that pressures in the base region of a blunt body at hypersonic speeds may be considerably greater than stream static pressure.

The afterbody-pressure level remains at about five to ten times stream pressure up to $\alpha = 20^\circ$; above $\alpha = 20^\circ$ the pressures on the windward side rapidly increase with increasing angle of attack. The pressures on the leeward side remain near ten times stream pressure throughout the angle-of-attack range of the tests. However, as pointed out in the preceding section, the pressures below $\alpha = 20^\circ$ are probably high. At $\alpha = 35^\circ$, when the afterbody cone generator on the most windward side ($\phi = 180^\circ$) has zero inclination to the main stream, pressures on the order of 40 times stream static pressure occur on the afterbody and increase up to 60 times stream static pressure at $\alpha = 40^\circ$. Pressures of this magnitude may have serious effects on aerodynamic heating and the overall aerodynamic forces.

CONCLUSIONS

On the basis of the results of the present investigation the following conclusions can be made:

1. Support-interference effects at very high Mach numbers can be significant and must be more fully investigated. Techniques to eliminate or to aid in the quantitative evaluation of these effects must be developed.

2. The pressure distribution over the model heat shield shows fair agreement with Newtonian theory throughout the angle-of-attack range, but the data indicate a strong pressure-relieving effect near the heat-shield corner.

3. On the afterbody, pressures from five to ten times stream static pressure were obtained with little change occurring in the angle-of-attack range between 0° and 20°. However, investigation of sting-diameter and sting-length effects have shown this value to be high.

4. At angles of attack greater than 20°, the afterbody pressures on the windward side of the model increased rapidly with increasing angle of attack. On the leeward side, little change was recorded throughout the angle-of-attack range.

Langley Research Center,
National Aeronautics and Space Administration,
Langley Station, Hampton, Va., March 15, 1963.

REFERENCES

1. Johnston, Patrick J., and Snyder, Curtis D.: Static Longitudinal Stability and Performance of Several Ballistic Spacecraft Configurations in Helium at a Mach Number of 24.5. NASA TN D-1379, 1962.

2. Mueller, James N.: Equations, Tables, and Figures for Use in the Analysis of Helium Flow at Supersonic and Hypersonic Speeds. NACA TN 4063, 1957.

3. Erickson, Wayne D.: Real-Gas Correction Factors for Hypersonic Flow Parameters in Helium. NASA TN D-462, 1960.

4. Henderson, Arthur, Jr.: Investigation of the Flow Over Simple Bodies at Mach Numbers of the Order of 20. NASA TN D-449, 1960.

5. Romeo, David J.: Experimental Results of the Pressure Distribution on a Blunt-Nose Conical-Afterbody Lunar-Mission Spacecraft With Four Nose-Edge Radii for a Mach Number of 6.0 and an Angle-of-Attack Range of 0° to 50°. NASA TM X-705, 1962.

6. Chapman, Dean R.: An Analysis of Base Pressure at Supersonic Velocities and Comparison With Experiment. NACA Rep. 1051, 1951. (Supersedes NACA TN 2137.)

7. Ferri, Antonio, and Pallone, Adrian: Note on the Flow Fields on the Rear Part of Blunt Bodies in Hypersonic Flow. WADC Tech. Note 56-294, U.S. Air Force, July 1956.

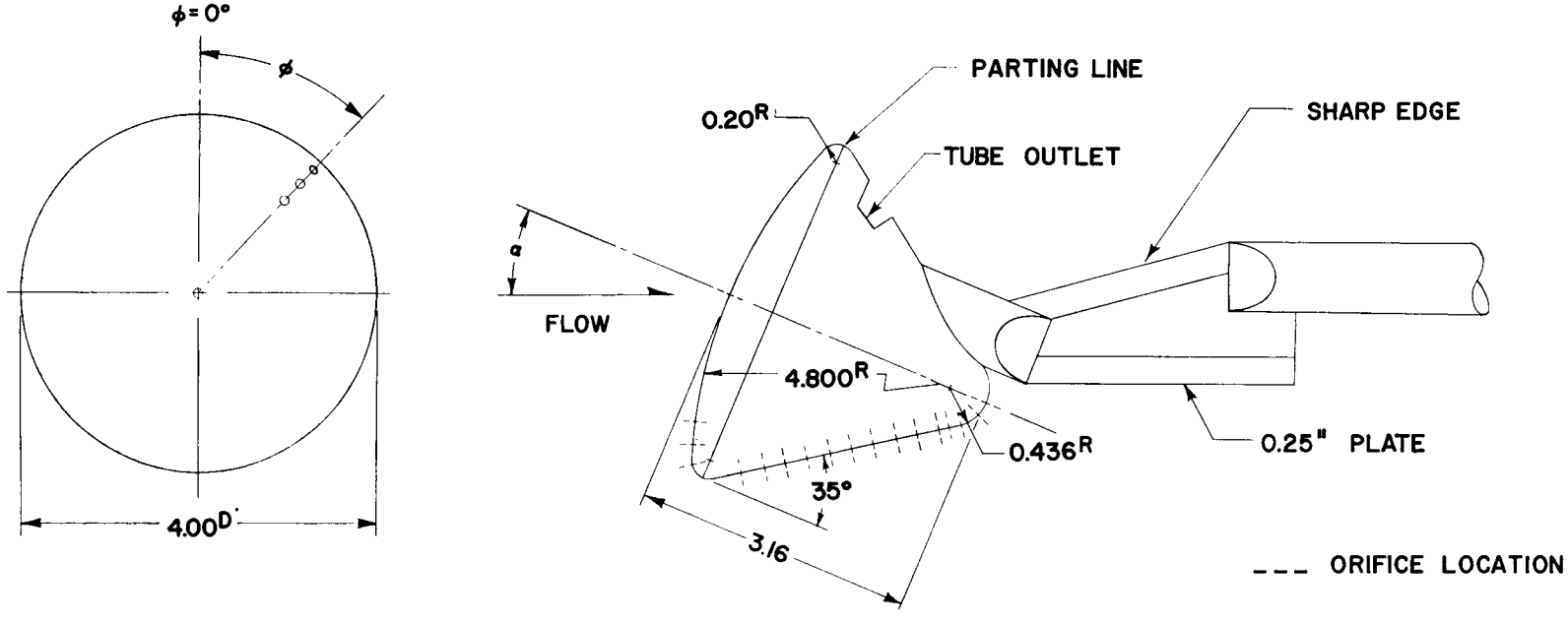

(a) 4-inch-diameter model.

Figure 1.- Models tested.

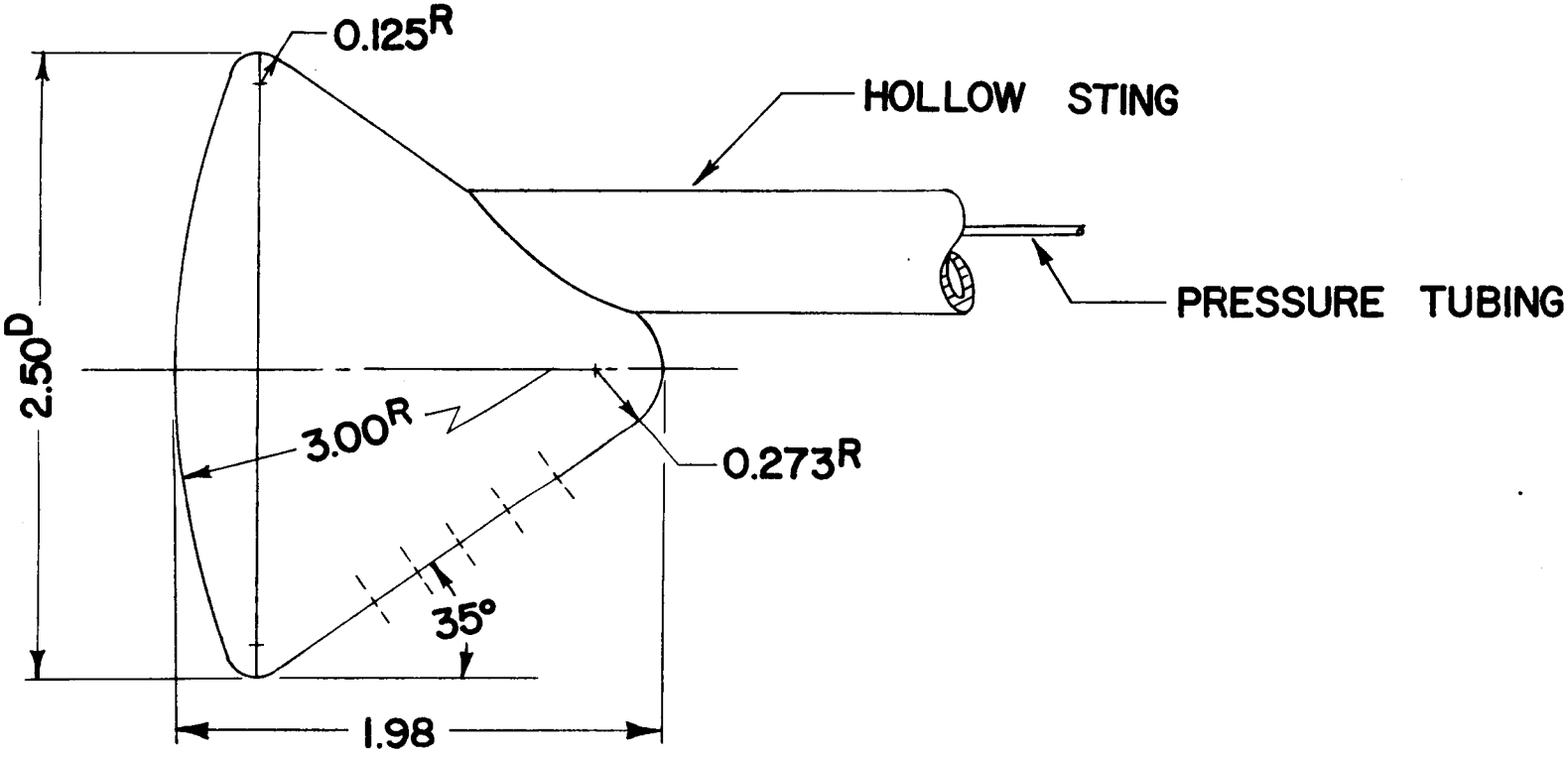

(b) $2\frac{1}{2}$-inch-diameter model.

Figure 1.- Continued.

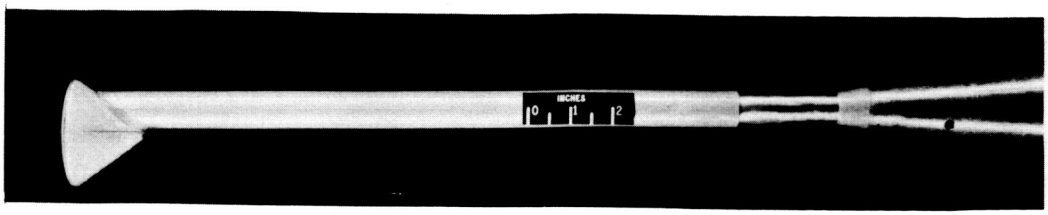

$\frac{d_s}{d} = 0.35$

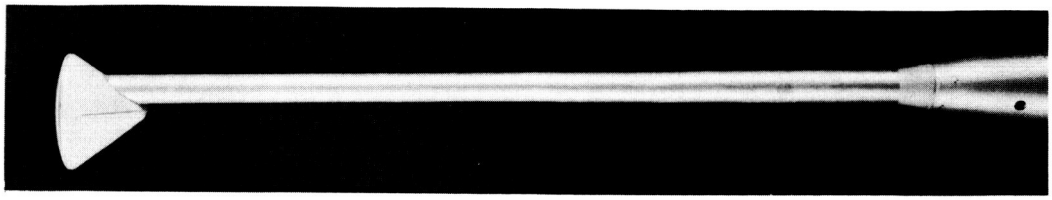

$\frac{d_s}{d} = 0.25$

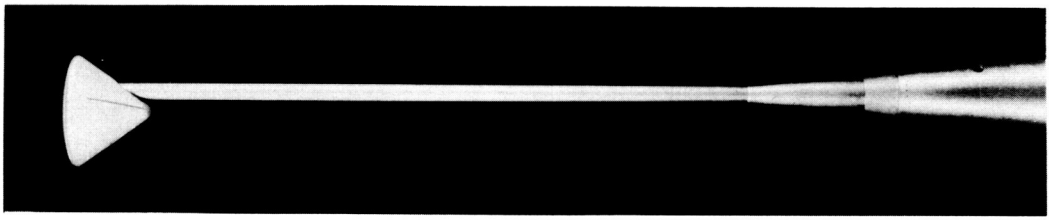

$\frac{d_s}{d} = 0.15$

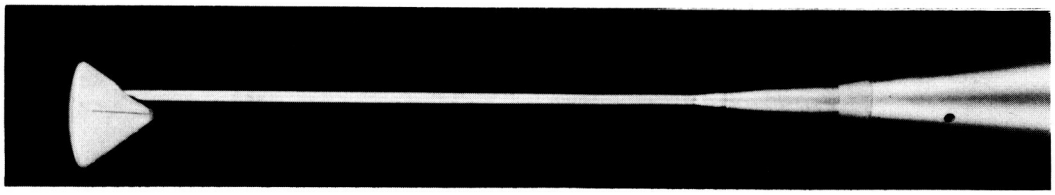

$\frac{d_s}{d} = 0.10$

(c) Photographs of $2\frac{1}{2}$-inch-diameter model. L-63-80

Figure 1.- Concluded.

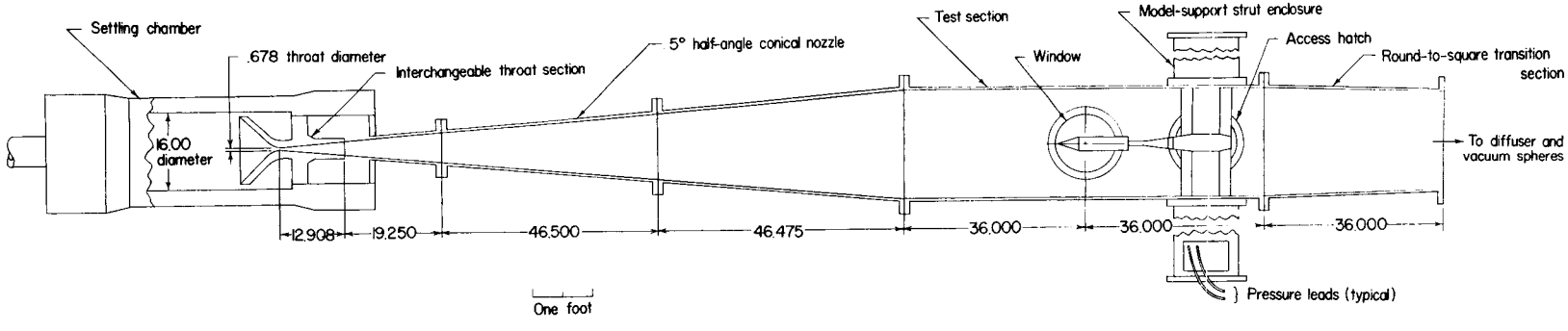

Figure 2.- Schematic diagram of the Langley 22-inch hypersonic helium tunnel. (All dimensions in inches unless otherwise noted.)

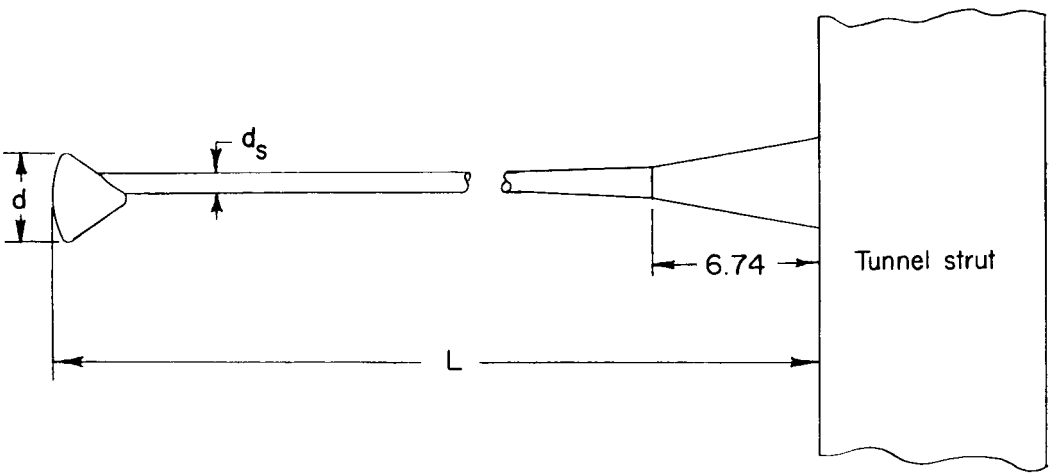

Figure 3.- Sting mount for $2\frac{1}{2}$-inch-diameter model.

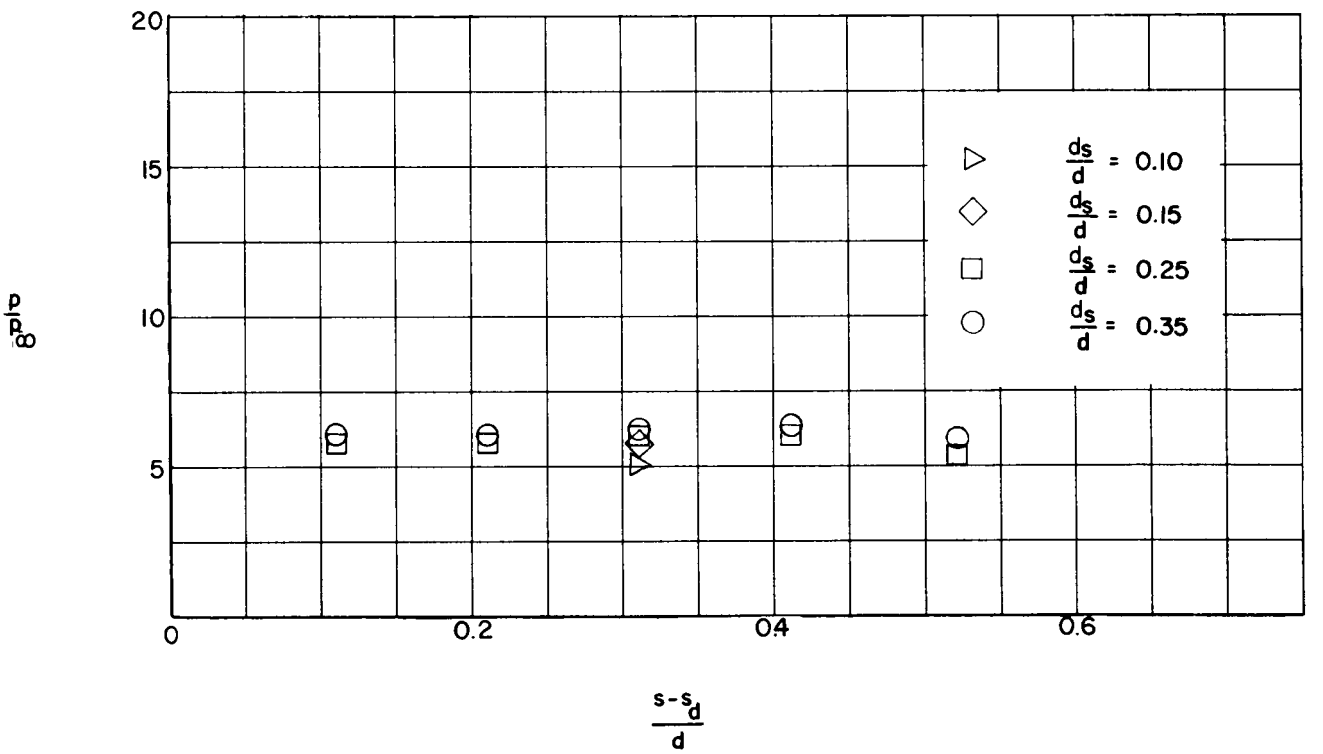

Figure 4.- Effect of sting diameter on afterbody pressure. Model diameter = $2\frac{1}{2}$ in.; L = 22.74 in.; M = 19.4.

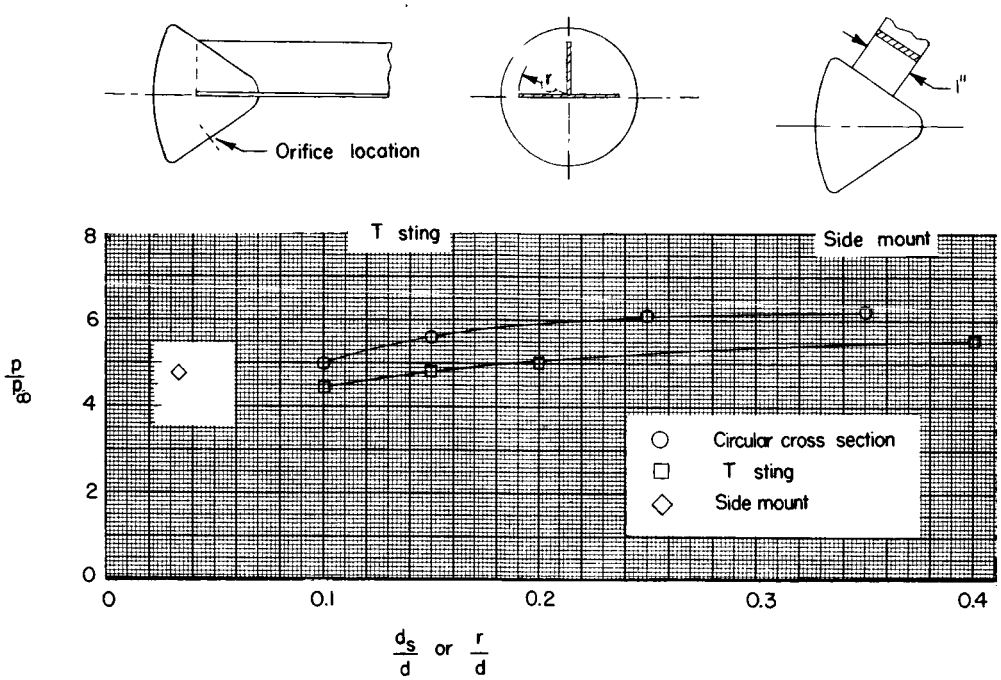

Figure 5.- Pressure ratios for different sting diameters at $\frac{s - s_a}{d} = 0.31$. Model diameter = $2\frac{1}{2}$ in.; L = 22.74 in.; M = 19.4.

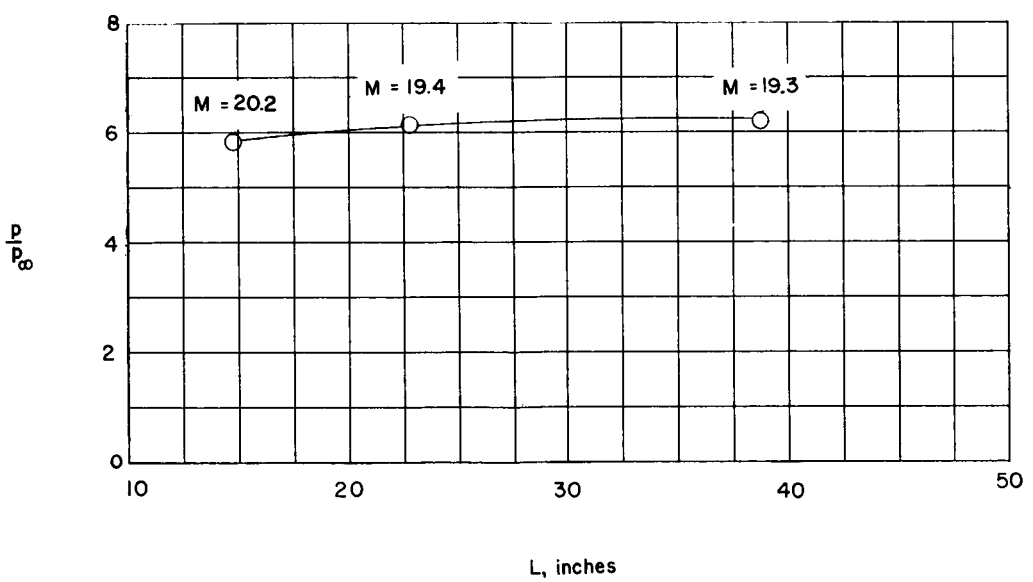

Figure 6.- Afterbody pressure ratios for different sting lengths. Model diameter = $2\frac{1}{2}$ in.; $\frac{d_s}{d} = 0.25$.

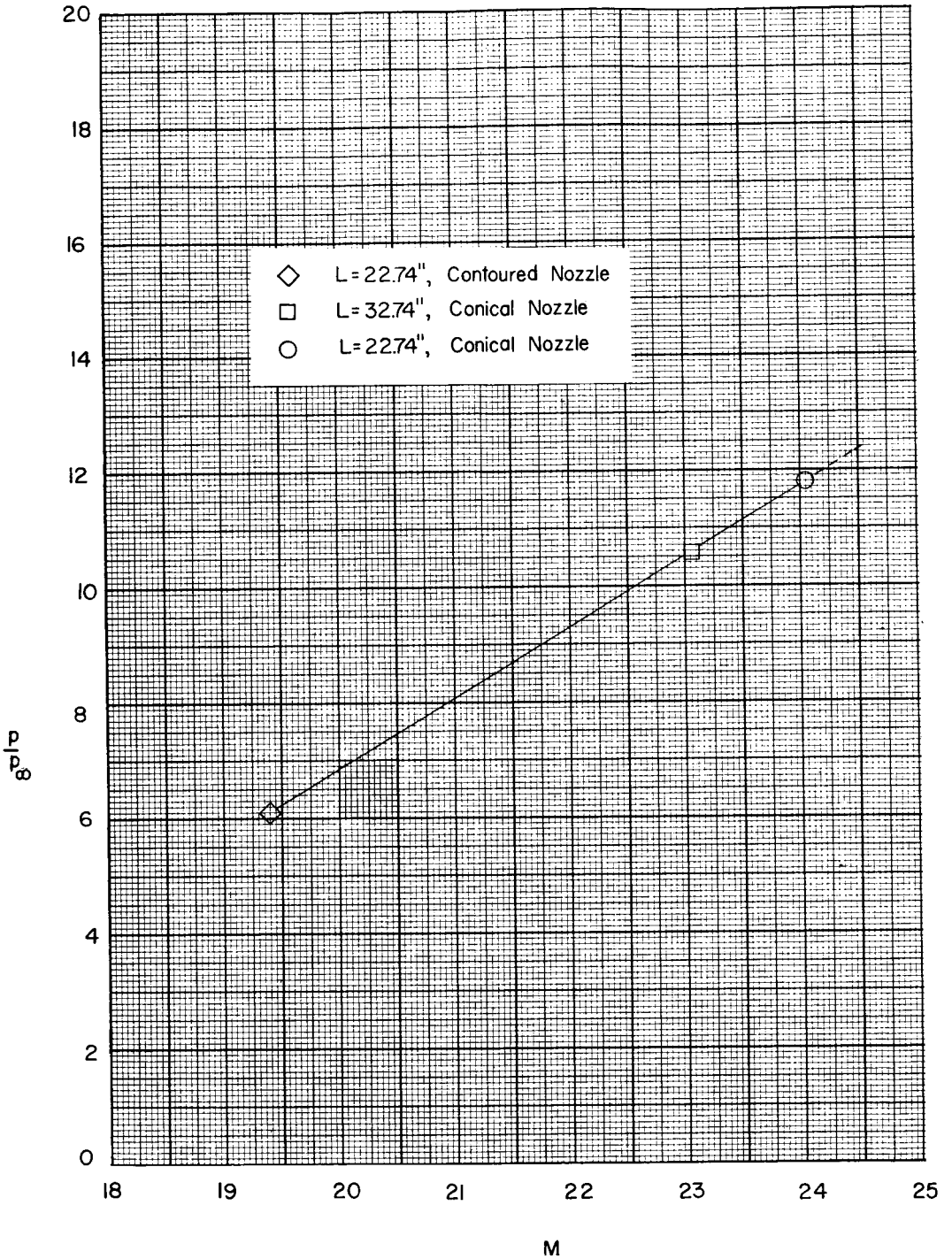

Figure 7.- Variation of afterbody pressure with free-stream Mach number. Model diameter= $2\frac{1}{2}$ in.; $\frac{d_s}{d} = 0.25$.

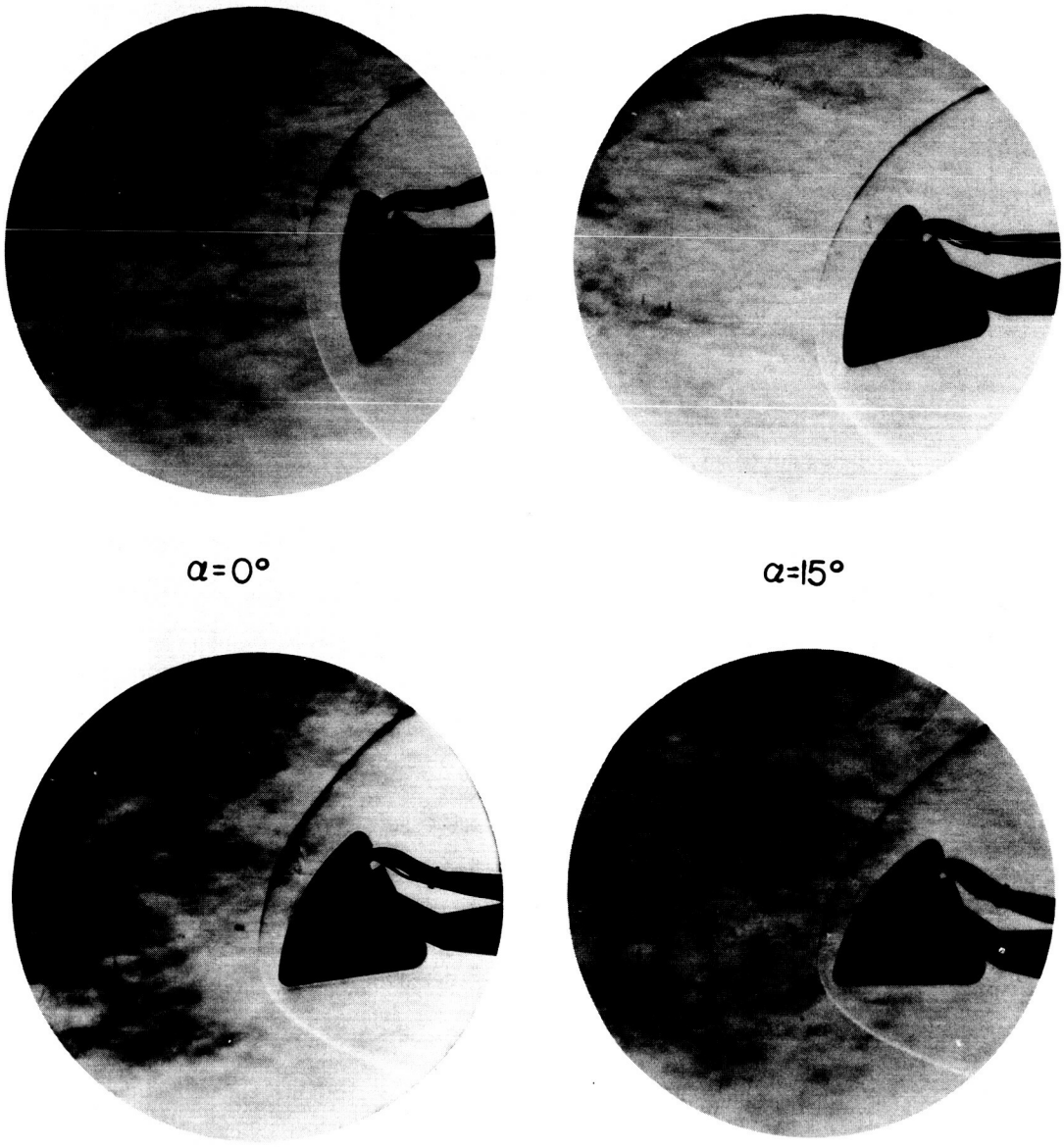

Figure 8.- Schlieren photographs of 4-inch-diameter model. M = 24.5; R = 1.18×10^6. L-63-81

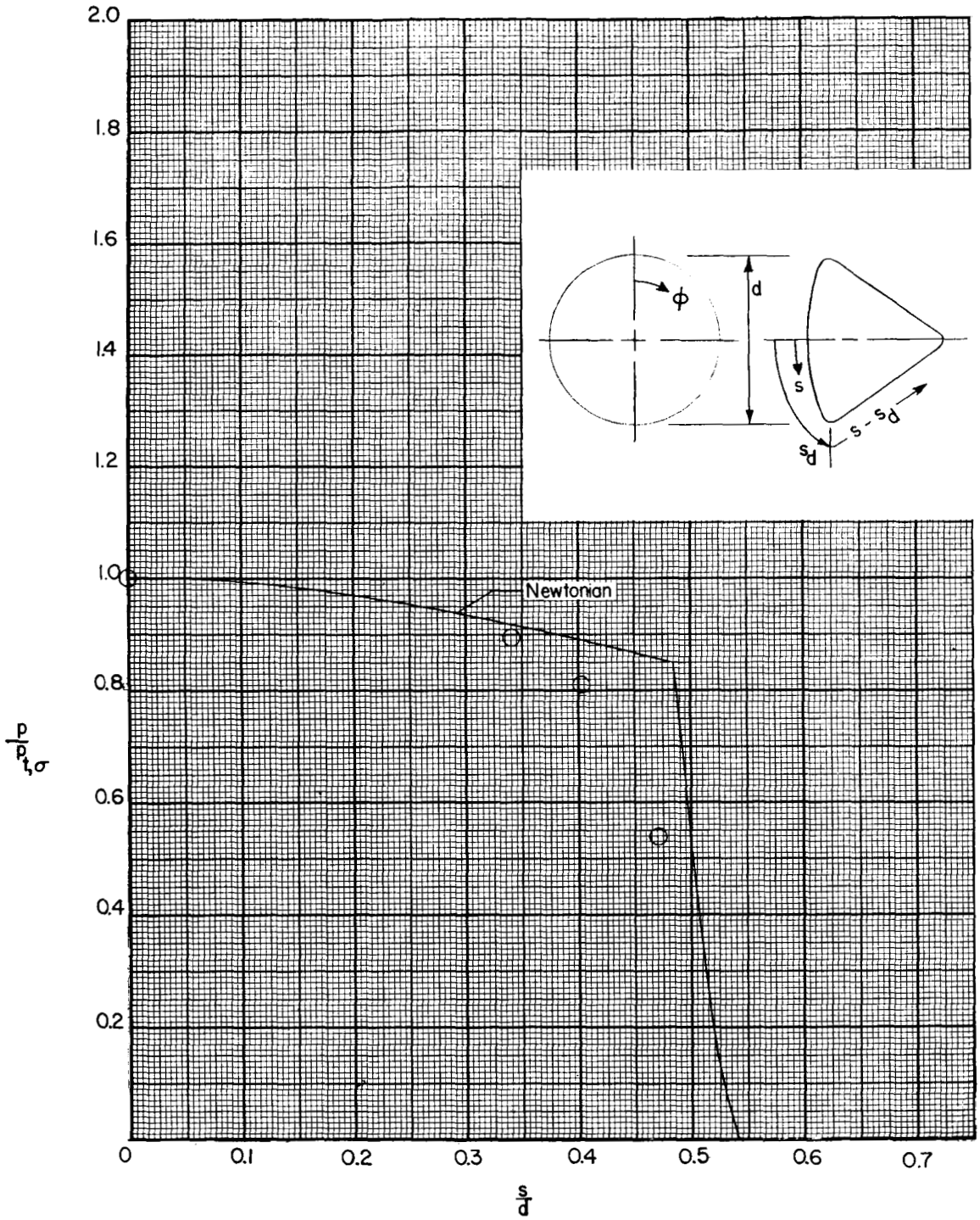

Figure 9.- Pressure distribution on heat shield at $\alpha = 0^{\circ}$. Model diameter = 4 in.; $M = 24.5$; $R = 1.18 \times 10^6$.

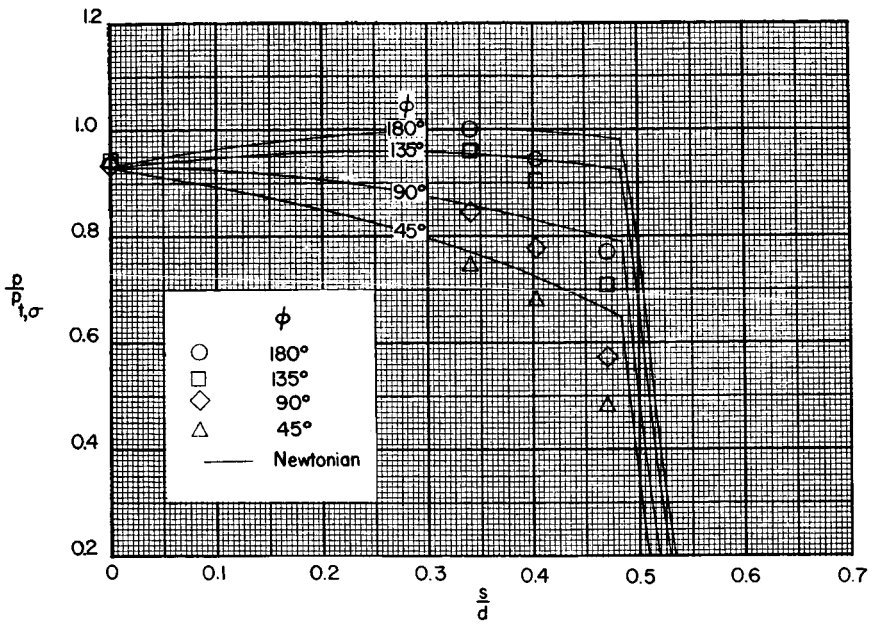

(a) $\alpha = 15^{\circ}$.

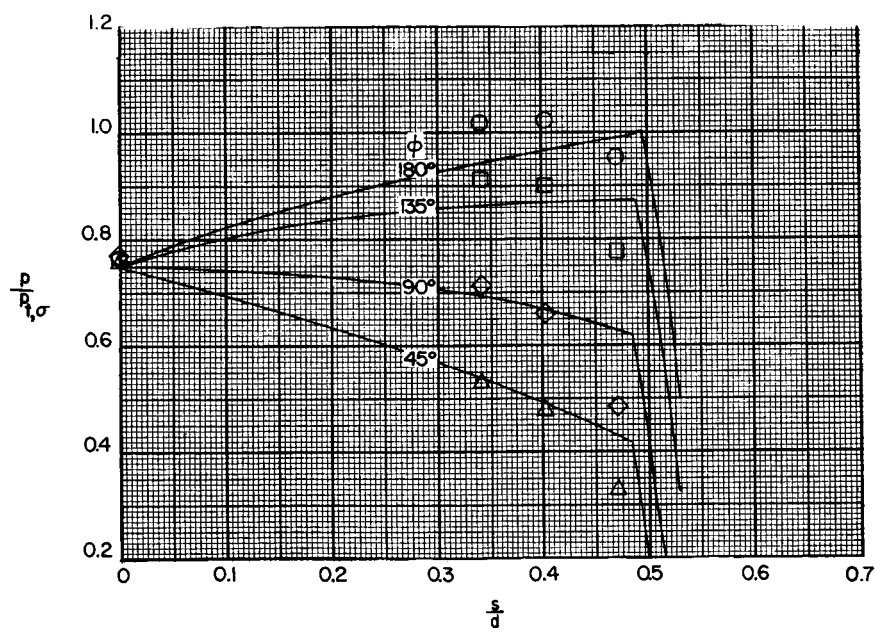

(b) $\alpha = 30^{\circ}$.

Figure 10.- Pressure distribution on heat shield at angles of attack. Model diameter = 4 in.; M = 24.5; R = 1.18×10^{6}.

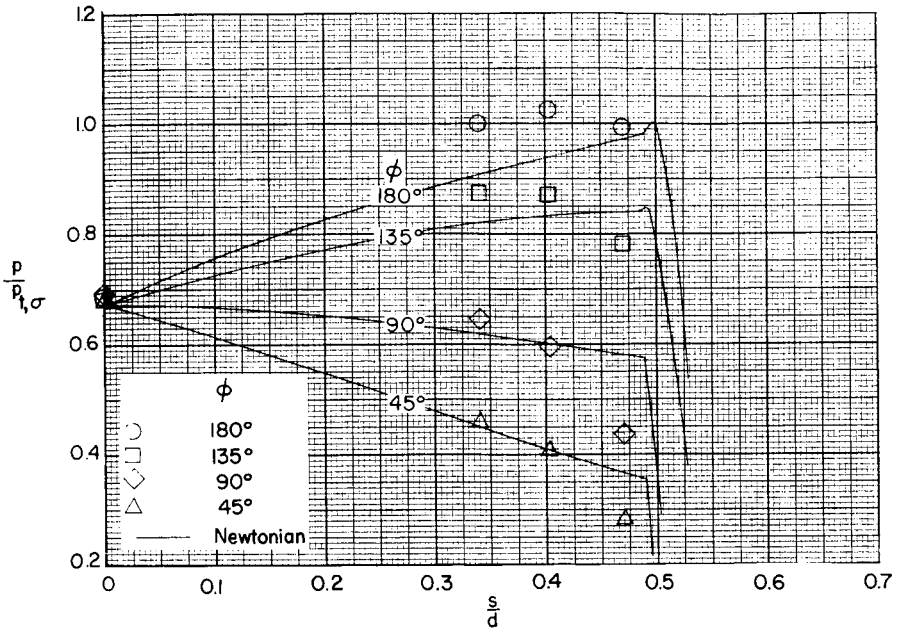

(c) $\alpha = 35^{\circ}$.

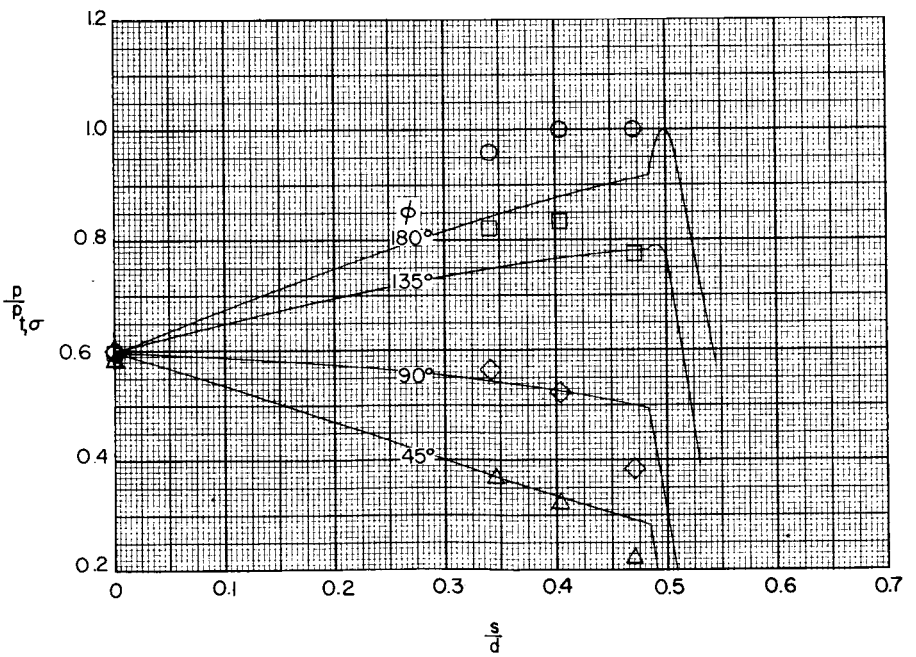

(d) $\alpha = 40^{\circ}$.

Figure 10.- Concluded.

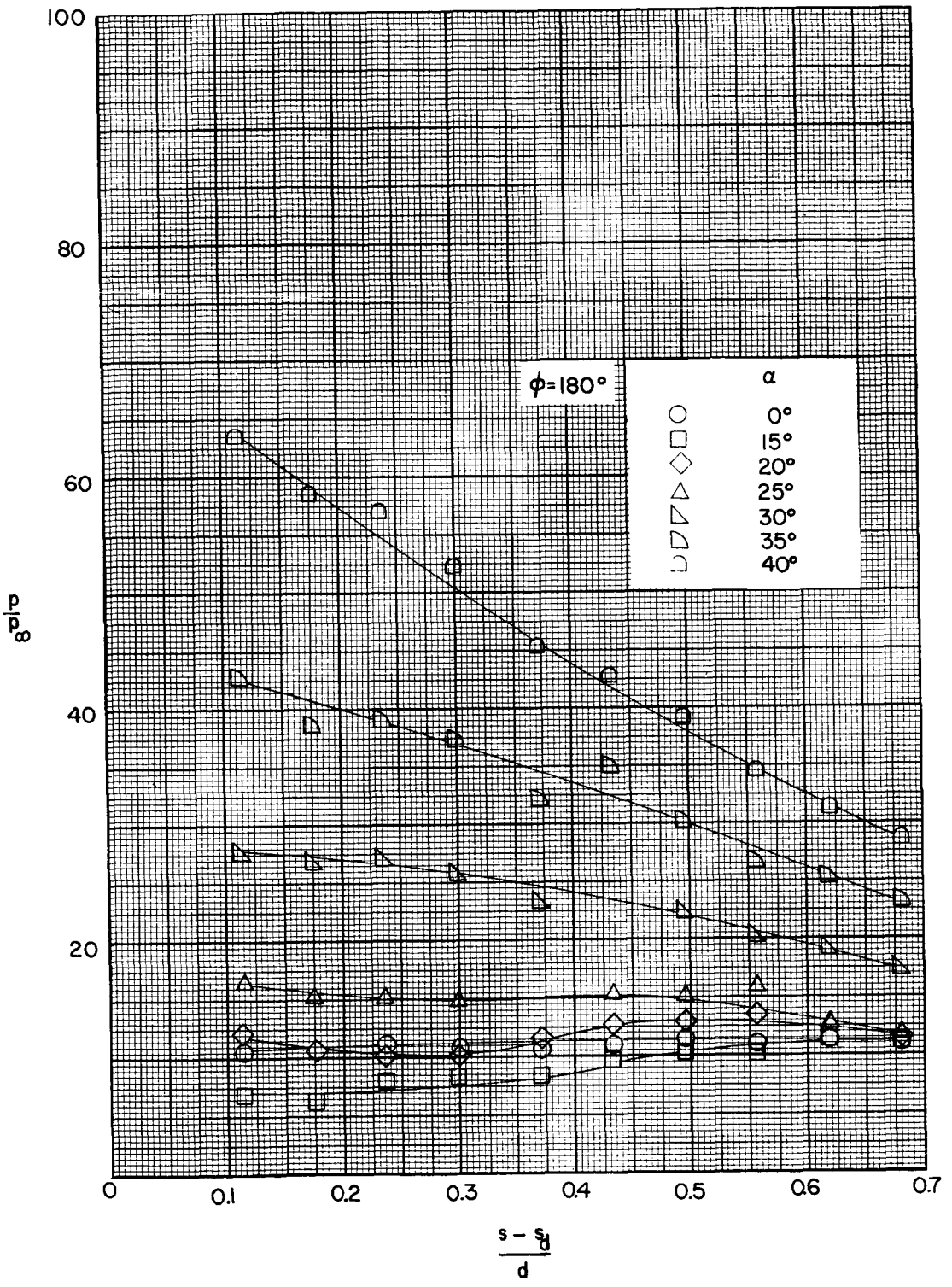

Figure 11.- Pressure distribution on afterbody at angles of attack. Model diameter = 4 in.; M = 24.5; R = 1.18×10^6.

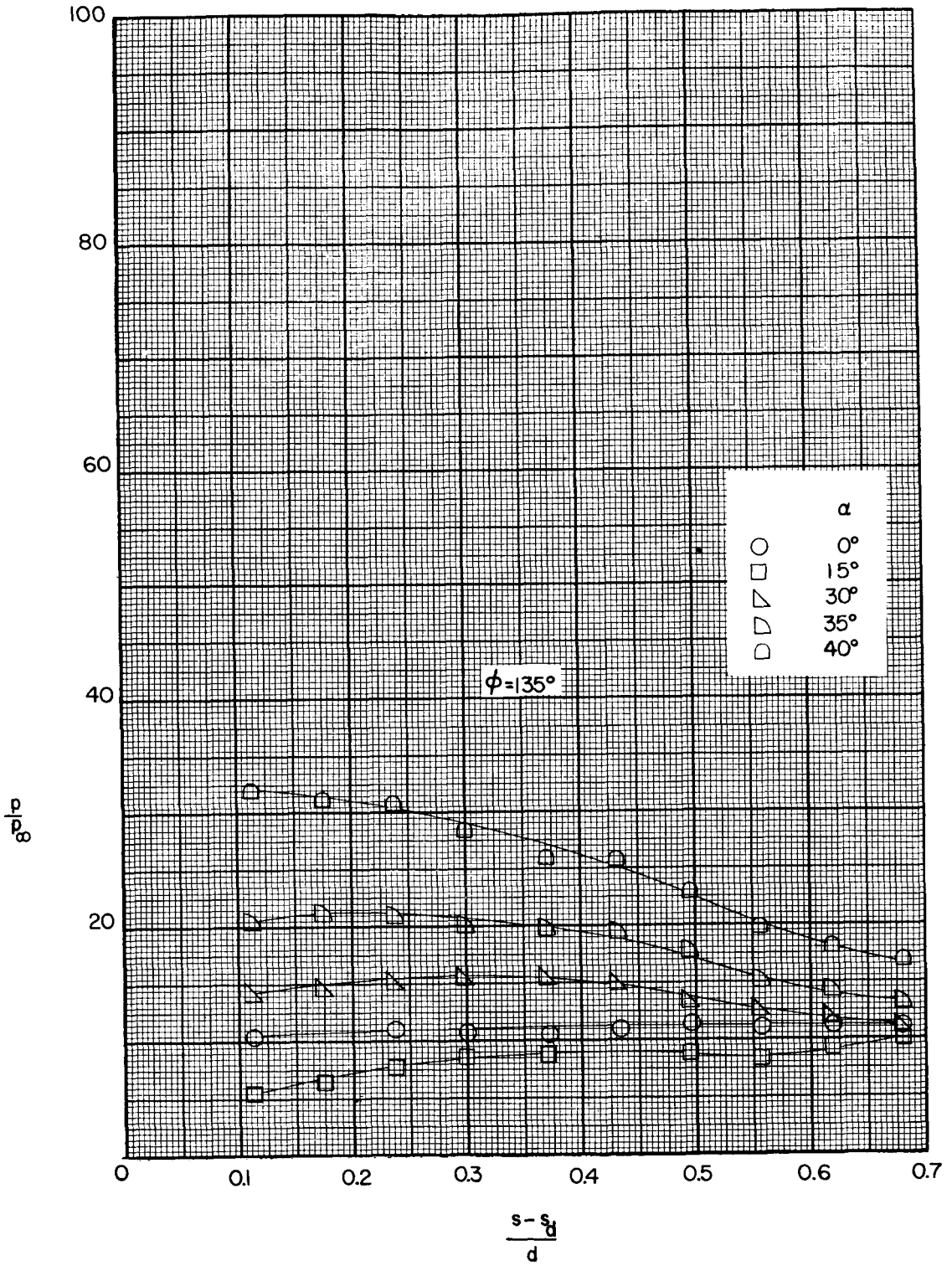

Figure 11.- Continued.

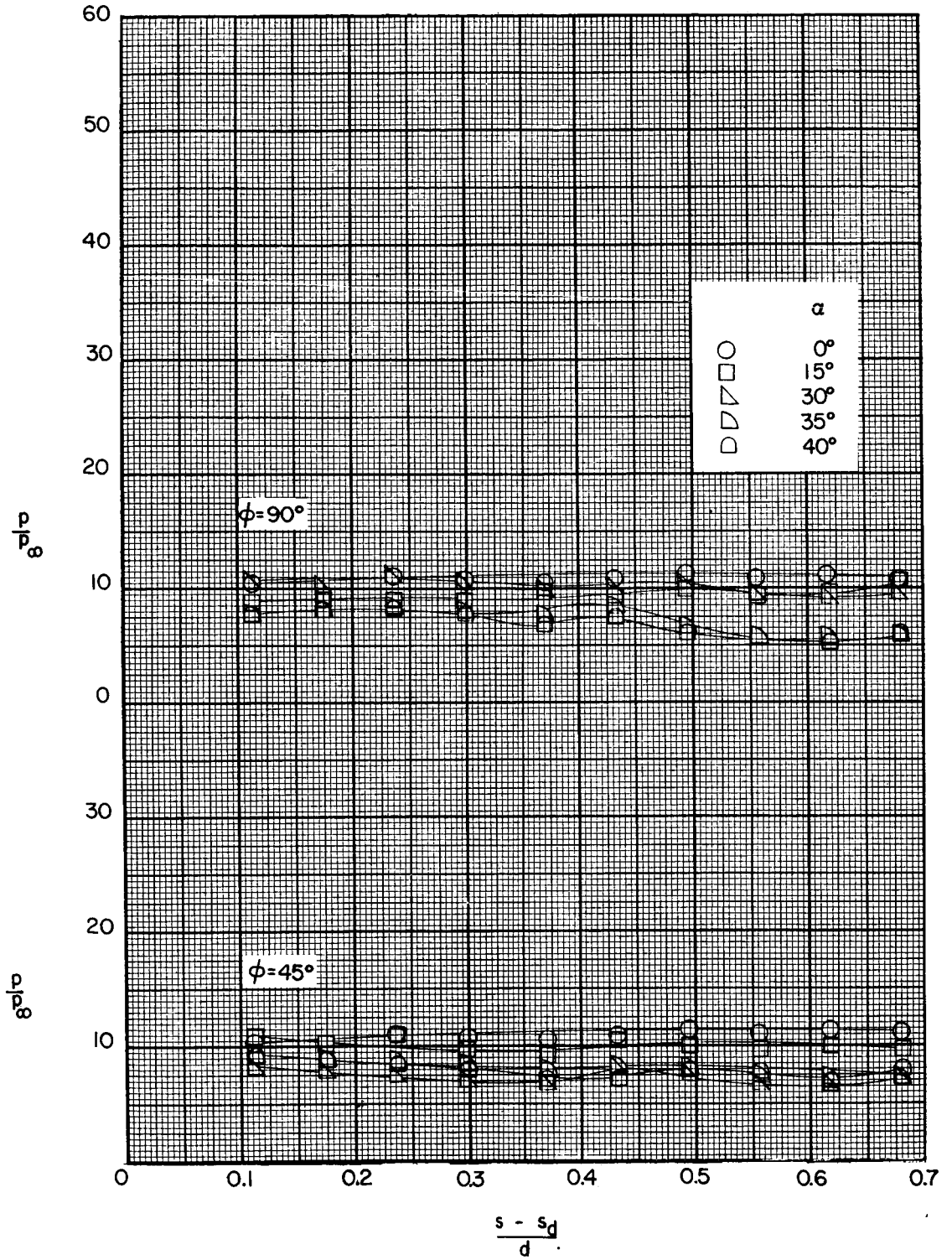

Figure 11.- Concluded.